JOURNAL OF PROPULSION AND POWER
Vol. 9, No. 3, May–June 1993

Nonreflecting Boundary Conditions of Three-Dimensional Euler Equation Calculations for Strut Cascades

K. Imanari* and H. Kodama†
Ishikawajima-Harima Heavy Industries, Tokyo, Japan

In this article, three-dimensional nonreflecting boundary conditions regarding pressure waves and associated components in density and velocity waves have been formulated and applied to time-marching Euler equation calculations of steady flows around uncambered thick strut cascades. The linearized solutions including a Fourier-Bessel double expansion with an exponential variation in the axial direction have been developed for far-field perturbations from the uniform freestream with subsonic axial velocity in a cylindrical annular duct, and used to provide the information for the correction of boundary conditions. Numerical examples for the symmetric struts, and the nonuniform strut cascades comprising two types of vanes, have demonstrated the correctness and accuracy of the present method, allowing a considerable reduction of the computational domain.

Nomenclature

a_0 = velocity of sound
C = complex coefficient of pressure perturbation
C_p = static pressure coefficient, pressure perturbation/(inlet stagnation pressure—mean static pressure)
h = hub-to-tip radius ratio
i = $\sqrt{-1}$
M_{ave} = circumferentially averaged Mach number
M_{isen} = isentropic Mach number along blade surface or midpitch line
M_0 = Mach number of mean flow averaged both in the circumferential and radial directions
N, L = number of circumferential and radial retained terms in a Fourier-Bessel finite double series
p_0, p = mean and perturbation components of static pressure
r = coordinate in radial direction
t = time
u_r = perturbation components of radial velocity
u_0, u_z = mean and perturbation components of axial velocity
u_θ = perturbation components of tangential velocity
z = coordinate in axial direction
δp = numerical pressure perturbation from the mean pressure p_0
θ = dimensionless coordinate in tangential direction
κ = ratio of specific heats
λ = eigenvalues of pressure wave
ρ_0, ρ = mean and perturbation components of density
ω = circular frequency

Subscripts
in = upstream boundary location
out = downstream boundary location
ln = lth radial and nth circumferential mode
0 = mean quantity averaged both in the circumferential and radial directions of flow variable

Received May 13, 1992; presented as Paper 92-3045 at the AIAA/SAE/ASME/ASEE 28th Joint Propulsion Conference and Exhibit, Nashville, TN, July 6–8, 1992; revision received Oct. 26, 1992; accepted for publication Dec. 18, 1992.

*Research Engineer, Research and Development Department, Aero-engine and Space Operations.
†Manager, Research and Development Department, Aero-engine and Space Operations.

Introduction

IN the steady numerical calculations of turbomachinery flows with subsonic axial velocities, upstream and downstream boundaries are located at a finite distance from the cascade, whereas the boundary conditions commonly used in the calculation are based on the conditions which should be ideally achieved at infinity, such as uniform flow variables and zero streamwise gradient in the flow properties. Consequently, nonphysical reflections of the flow disturbances propagated from the cascade may occur at the boundaries in greater or lesser degree. In order to eliminate the effect of nonphysical reflections on numerical solutions, the distance from the cascade to an upstream or downstream boundary has to be large enough to attenuate the flow disturbances at the boundaries to an acceptable level.

For the case of strut cascades, such as bypass strut/pylon in a turbofan engine, the pressure perturbations induced by the vanes are so large that computational domains of considerable size for both upstream and downstream regions are required to perform three-dimensional flow calculations properly. One of the answers to this problem would be an application of nonreflecting boundary conditions which prevent nonphysical reflections from being produced at the boundaries, so that the computational domain can be reduced with little disturbance of the correct flow solution. This leads to greater computational efficiency.

Verdon and Casper[1] have developed the upstream and downstream boundary conditions which consider outgoing pressure waves in the far field for unsteady aerodynamic calculations on two-dimensional cascades using the linearized potential equations. Whitehead[2] used a similar approach for both unsteady and steady potential flow calculations around two-dimensional cascades. These ideas were extended to the two-dimensional linearized Euler equations for unsteady cascade flows by Hall and Crawley.[3]

Ferm and Gustafsson[4] derived the boundary conditions for steady inviscid flow calculations of a two-dimensional duct, using the solutions of the linearized Euler equations. A similar method was developed by Hirsch and Verhoff[5] for two-dimensional uncambered cascade flows. They have shown that their method can reduce the computational domain considerably, while keeping the accuracy. Giles[6] formulated both unsteady and steady nonreflecting boundary conditions for two-dimensional time-dependent Euler equation calculations.

He performed steady flow calculations of a turbine cascade, showing fair savings in computational meshes. His method accounted for the incoming waves due to nonphysical reflections. After separation of numerical perturbations at the boundaries into incoming and outgoing modes by the relation between one-dimensional characteristic and primitive variables [see (5.9) and (5.10) of Ref. 7], the former modes were removed to avoid nonphysical reflections. Saxer and Giles[8] applied the quasi-three-dimensional nonreflecting boundary conditions to three-dimensional steady calculations of a transonic axial flow turbine stage, including the mixing plane at the stator/rotor interface. This method may be useful if the blade pitch is much smaller than the tip radius, but would produce some errors when calculating a flow around typical strut cascades on which the blade pitch is comparable with the tip radius.

In this article, a method to treat the boundary conditions for three-dimensional time-marching Euler equation calculations of steady flows around uncambered thick strut cascades has been developed in order to accept boundaries much closer to the cascades. The size of the computational grids is thereby reduced. The three-dimensional linearized solutions regarding pressure waves and associated components in density and velocity waves have been formulated for far-field perturbations from the uniform freestream with subsonic axial velocity in a cylindrical annual duct, and used to provide the information for the correction of boundary conditions. The construction of nonreflecting boundary conditions begins by decomposition of numerical solutions into the incoming and outgoing waves for each flow variable at the boundaries by using the linearized solutions. The correction of boundary conditions is made by removing the incoming pressure waves and associated quantities. Numerical examples for the symmetric struts and the nonuniform strut cascades comprising two types of vanes are shown to confirm the validation of the present method.

Formulation

Consider three-dimensional time-dependent Euler equations to calculate steady flows around uncambered strut cascades in a coaxial cylindrical duct of infinite axial extent. The governing equations can be linearized near upstream and downstream boundaries if it is assumed that the perturbation quantities of flow variables are small compared to the mean quantities averaged both in the circumferential and radial directions. The resultant equations are

Continuity

$$\frac{D\rho}{Dt} + \rho_0 \nabla \cdot \boldsymbol{u} = 0 \tag{1}$$

Momentum

$$\frac{D\boldsymbol{u}}{Dt} = -\frac{1}{\rho_0} \nabla_p \tag{2}$$

Energy

$$\frac{D\rho}{Dt} = \frac{1}{a_0^2} \frac{Dp}{Dt} \tag{3}$$

where length scale is normalized by the tip radius. The vector $\boldsymbol{u}$ is the form of velocity perturbations defined by

$$\boldsymbol{u} = (u_\theta, u_z, u_r) \tag{4}$$

a_0 indicates the velocity of sound defined by

$$a_0 = \sqrt{(\kappa p_0/\rho_0)} \tag{5}$$

D/Dt represents the substantive derivative defined by

$$\frac{D}{Dt} = \frac{\partial}{\partial t} + u_0 \frac{\partial}{\partial z} \tag{6}$$

Furthermore, ∇ is the differential operator defined by

$$\nabla = \left(\frac{\partial}{r\partial\theta}, \frac{\partial}{\partial z}, \frac{\partial}{\partial r} \right) \tag{7}$$

The following equations are derived from Eqs. (1–3):

$$\nabla^2 p - \frac{1}{a_0^2} \frac{D^2 p}{Dt^2} = 0 \tag{8}$$

$$\frac{D}{Dt} (\nabla \times \boldsymbol{u}) = 0 \tag{9}$$

$$\frac{Ds}{Dt} = \frac{D}{Dt} \left(\frac{p}{p_0} - \kappa \frac{\rho}{\rho_0} \right) = 0 \tag{10}$$

Equation (8) indicates the acoustic wave equation in the convective systems. Equations (9) and (10) mean that vorticity and entropy are convected downstream by the mean axial velocity u_0, respectively.

The perturbation in pressure is assumed to be

$$p = \sum_{l=0}^{\infty} \sum_{n=0}^{\infty} CR_l^{(n)}(r) \exp(\lambda z) \exp(i\omega t + in\theta) \tag{11}$$

where $R_l^{(n)}(r)$ is a complete set of orthonormal radial eigenfunctions. The eigenfunction $R_l^{(n)}(r)$ is constructed as normalized combinations of the Bessel functions of the first and second kinds of order n. They are obtained as a solution to

$$\frac{d^2 R_l^{(n)}(r)}{dr^2} + \frac{1}{r} \frac{dR_l^{(n)}(r)}{dr} + \left(k_l^{(n)^2} - \frac{n^2}{r^2} \right) R_l^{(n)}(r) = 0 \tag{12a}$$

$$\frac{dR_l^{(n)}(r)}{dr} = 0 \quad \text{at} \quad r = h \quad \text{and} \quad 1 \tag{12b}$$

$$\int_h^1 r R_l^{(n)}(r) R_m^{(n)}(r)\, dr = \delta_{lm} \tag{12c}$$

where $k_l^{(n)}$ is the corresponding radial eigenvalues and δ_{lm} denotes Kronecker delta.

Substitution of the assumed solution of p into Eq. (8) gives the axial eigenvalues

$$\lambda_{1ln}, \lambda_{2ln} = \frac{i(\omega/a_0)M_0 \pm \sqrt{(1 - M_0^2)k_l^{(n)} - (\omega/a_0)^2}}{1 - M_0^2} \tag{13}$$

Therefore, the pressure perturbation is given as

$$p = \sum_{l=0}^{\infty} \sum_{n=0}^{\infty} R_l^{(n)}(r) \exp(i\omega t + in\theta) [C_{1ln} \exp(\lambda_{1ln} z) + C_{2ln} \exp(\lambda_{2ln} z)] \tag{14}$$

Equation (14) shows that the pressure field is constructed of two waves, one of which attenuates in the upstream direction (λ_1) and the other in the downstream (λ_2) for subsonic flows.

The potential components in the velocity waves and density wave, which are associated with pressure waves, can be de-

scribed by

$$\begin{pmatrix}\rho\\ u_\theta\\ u_z\\ u_r\end{pmatrix} = \sum_{l=0}^{\infty}\sum_{n=0}^{\infty}\left\{ C_{1ln}\begin{bmatrix} \dfrac{R_l^{(n)}(r)}{a_0^2} \\ \dfrac{-inR_l^{(n)}(r)}{\rho_0 r(i\omega + u_0\lambda_{1ln})} \\ \dfrac{-\lambda_{1ln}R_l^{(n)}(r)}{\rho_0(i\omega + u_0\lambda_{1ln})} \\ \dfrac{-\mathrm{d}R_l^{(n)}(r)}{\mathrm{d}r} \Big/ \rho_0(i\omega + u_0\lambda_{1ln}) \end{bmatrix} \exp(\lambda_{1ln}z) \right.$$

$$\left. + C_{2ln}\begin{bmatrix} \dfrac{R_l^{(n)}(r)}{a_0^2} \\ \dfrac{-inR_l^{(n)}(r)}{\rho_0 r(i\omega + u_0\lambda_{2ln})} \\ \dfrac{-\lambda_{2ln}R_l^{(n)}(r)}{\rho_0(i\omega + u_0\lambda_{2ln})} \\ \dfrac{-\mathrm{d}R_l^{(n)}(r)}{\mathrm{d}r} \Big/ \rho_0(i\omega + u_0\lambda_{2ln}) \end{bmatrix} \exp(\lambda_{2ln}z) \right\} \exp(i\omega t + in\theta) \tag{15}$$

The plane wave represented by $(l, n) = (0, 0)$ is excluded from the perturbation quantities.

Numerical experience indicates that ω can be assumed zero for steady flow calculations in the time-marching procedure, since a flow solution at every time step can be approximated to be quasisteady as long as there is no source of unsteady incoming wave.

Reflecting Boundary Conditions

At the upstream boundary, four physical quantities such as stagnation pressure, stagnation temperature, yaw flow angle, and pitch flow angle are specified in the present analysis. They are held uniform in the circumferential direction. At the downstream boundary, static pressure is fixed uniform.

Nonreflecting Boundary Conditions

Upstream Boundary Conditions

This boundary condition begins by expanding the numerical perturbations of pressure δp and its gradient in the axial direction at the boundary into Fourier-Bessel double finite series as follows:

$$\delta p(r, \theta, z_{in}) = \sum_{l=0}^{L-1}\sum_{n=0}^{N-1} R_l^{(n)}(r)\exp(in\theta)[C_{1ln}\exp(\lambda_{1ln}z_{in}) + C_{2ln}\exp(\lambda_{2ln}z_{in})] \tag{16a}$$

$$\frac{\mathrm{d}\delta p}{\mathrm{d}z}(r, \theta, z_{in}) = \sum_{l=0}^{L-1}\sum_{n=0}^{N-1} R_l^{(n)}(r)\exp(in\theta)[C_{1ln}\lambda_{1ln}\cdot\exp(\lambda_{1ln}z_{in}) + C_{2ln}\lambda_{2ln}\exp(\lambda_{2ln}z_{in})] \tag{16b}$$

where δp and its gradient in the axial direction are extrapolated from the interior flowfield. These perturbation quantities involve both incoming and outgoing contributions. C_{1ln} is the amplitude for each mode of the outgoing pressure waves, and C_{2ln} is the amplitude for incoming waves. Rewriting Eqs. (16a) and (16b) into the form of each Fourier-Bessel mode with substitution of zero into z_{in}, leads to the simple expression of C_{1ln} and C_{2ln}, using the orthogonality condition [Eq. (12c)].

$$C_{1ln} = [(N_{ln} - \lambda_{2ln}M_{ln})/(\lambda_{1ln} - \lambda_{2ln})] \tag{17a}$$

$$C_{2ln} = [(M_{ln}\lambda_{1ln} - N_{ln})/(\lambda_{1ln} - \lambda_{2ln})] \tag{17b}$$

where M_{ln} and N_{ln} respectively denote the amplitudes described by Eqs. (18a) and (18b)

$$M_{ln} = \frac{1}{2\pi}\int_h^1 rR_l^{(n)}(r)\int_0^{2\pi}\delta p(r, \theta, 0)\exp(-in\theta)\,\mathrm{d}\theta\,\mathrm{d}r \tag{18a}$$

$$N_{ln} = \frac{1}{2\pi}\int_h^1 rR_l^{(n)}(r)\int_0^{2\pi}\frac{\mathrm{d}\delta p}{\mathrm{d}z}(r, \theta, 0)\exp(-in\theta)\,\mathrm{d}\theta\,\mathrm{d}r \tag{18b}$$

The incoming pressure waves and associated components in density and velocity waves are identified with nonphysical reflections at the upstream boundary, because there must be no incoming pressure perturbation in the present study. Therefore, they should be removed and the outgoing potential perturbations are considered at the boundary. The resulting equations can be expressed as

$$\begin{bmatrix}\rho\\ u_\theta\\ u_z\\ u_r\\ p\end{bmatrix} = \sum_{l=0}^{L-1}\sum_{k=0}^{K-1} C_{1ln}\begin{bmatrix} \dfrac{R_l^{(n)}(r)}{a_0^2} \\ \dfrac{-inR_l^{(n)}(r)}{\rho_0 r(i\omega + u_0\lambda_{1ln})} \\ \dfrac{-\lambda_{1ln}R_l^{(n)}(r)}{\rho_0(i\omega + u_0\lambda_{1ln})} \\ \dfrac{-\mathrm{d}_{ln}r_l^{(n)}(r)}{\mathrm{d}r} \Big/ \rho_0(i\omega + u_0\lambda_{1ln}) \\ R_l^{(n)}(r) \end{bmatrix} \exp(in\theta) \tag{19}$$

The mean quantities of density, axial velocity, and pressure at the boundary are obtained by averaging the numerical solutions, both in the circumferential and radial directions. Vorticity and entropy components can be considered into the boundary conditions if they are known at infinite upstream.

Downstream Boundary Conditions

The Fourier-Bessel expansions of both δp and its gradient in the axial direction at the boundary can be obtained in the same way as the upstream boundary conditions, except z_{out} replaces z_{in} in Eqs. (16a) and (16b). In contrast to the upstream boundary, C_{1ln} corresponds to an incoming mode, and C_{2ln} to an outgoing mode at the downstream.

Consequently, the final expression of pressure perturbation at the downstream boundary is

$$p = \sum_{l=0}^{L-1}\sum_{n=0}^{N-1} C_{2ln}R_l^{(n)}(r)\exp(in\theta) \tag{20}$$

The above perturbation is added to the mean pressure previously specified.

Numerical Examples

Numerical examples are provided for the symmetric struts and the nonuniform strut cascades comprising two types of vanes. The calculation conditions are shown in Table 1 for both of them. In the present examples, there was no perturbation in vorticity and entropy at infinite upstream. The Euler

Table 1 Symmetric and nonuniform struts

	Case 1	Case 2	Case 3
Inlet Mach number	0.52	0.52	0.52
Hub-to-tip radius	0.4	0.99	0.6
Large strut			
Blade number	11	4	4
Chord-to-tip radius	0.25	0.65	0.65
Max thickness-to-tip radius	0.075 (hub), 0.05 (tip)	0.13	0.1
Small strut			
Blade number		8	8
Chord-to-tip radius		0.325	0.25
Max thickness-to-tip radius		0.065	0.05
Grid			
Axially extended	21 × 91 × 21	31 × 71 × 3	31 × 71 × 11
Axially restricted	21 × 27 × 21	31 × 31 × 3	31 × 31 × 11

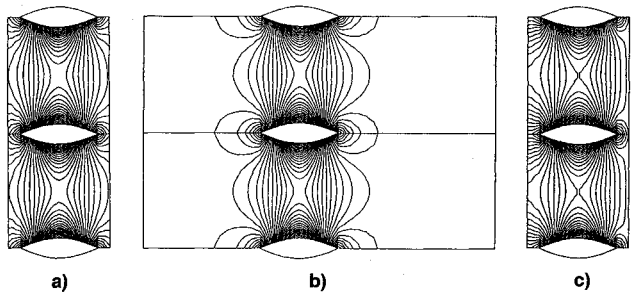

Fig. 1 Isopressure distribution at midspan for case 1 (increments between isopressure lines are 1% of inlet stagnation pressure): a) nonreflecting boundary conditions on restricted grid, b) reflecting boundary conditions on extended grid, and c) reflecting boundary conditions on restricted grid.

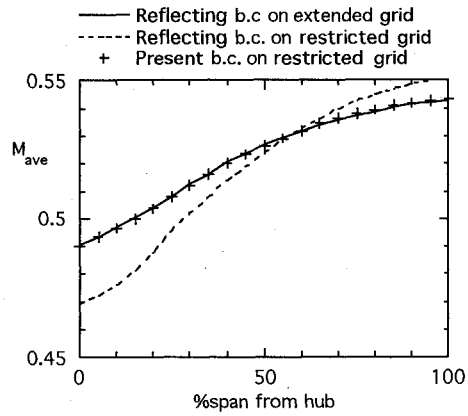

Fig. 2 Circumferentially mass-averaged Mach number distribution at the upstream boundary of restricted grid for case 1.

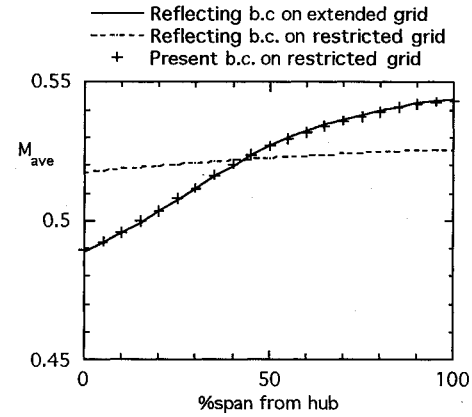

Fig. 3 Circumferentially mass-averaged Mach number distribution at the downstream boundary of restricted grid for case 1.

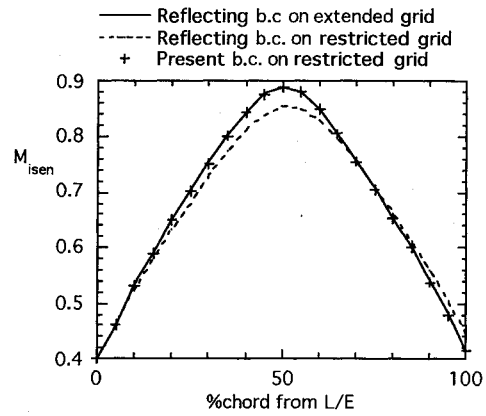

Fig. 4 Isentropic blade surface Mach number distribution at midspan for case 1.

solver based on Denton's explicit scheme,[9] applying finite volume formulation, was used to obtain steady flow solutions on a time-marching procedure.

In case 1, relatively low hub-to-tip radius ratio of 0.4 and a strut configuration with radially varied thickness were chosen to produce a highly three-dimensional pressure field. Figure 1 shows the isopressure distribution at the midspan, comparing the results obtained for the extended and restricted domains, the latter with the corrected boundary treatment. As noticed by the unsymmetrical distribution in Fig. 1c, the static pressure field was affected by the reflecting boundary conditions. The level of error at the boundaries was 4–5% of the inlet stagnation pressure, compared to Fig. 1b which was a reference result on the axially extended grid. On the other hand, when the nonreflecting boundary conditions were introduced (Fig. 1a) a symmetric distribution was clearly obtained even with the restricted computational region. Figures 2 and 3 show the spanwise distribution of circumferentially mass-averaged Mach number. It is seen in the figures that the radial distribution was also affected by the nonphysical reflections. A good agreement was obtained in the results between the reference computation on the extended grid and the calculation with the corrected boundary treatment, even though the latter used the restricted gird. Conversely, the results using the reflecting boundary conditions on the restricted grid involved an error of 0.02–0.03 in Mach number at both endwalls. Figures 4 and 5 show the axial distribution of isentropic Mach number on blade surface and midpitch line at the midspan, respectively. The error of 0.03–0.04 in blade surface Mach number, due to the nonphysical reflections, was removed almost completely by the use of the present boundary treatment.

Figure 6 shows the extended and restricted computational grids for the nonuniform struts of case 2, where a nearly two-dimensional flowfield was produced by setting hub-to-tip ra-

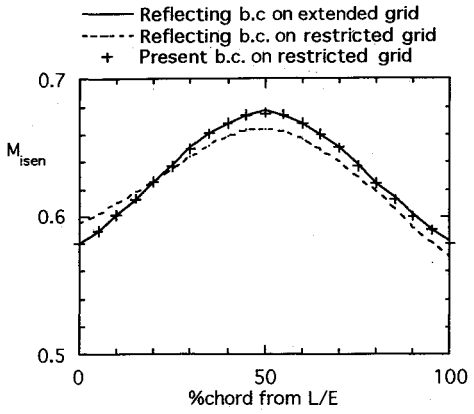

Fig. 5 Isentropic midpitch Mach number distribution at midspan for case 1.

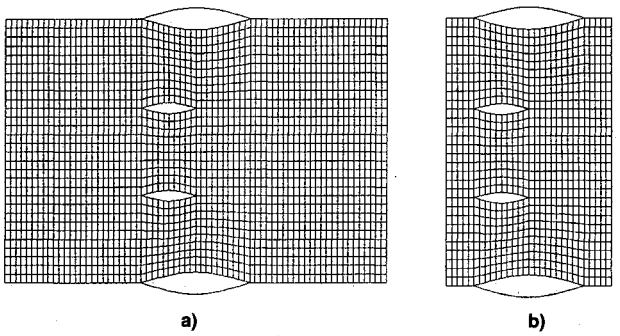

Fig. 6 Computational grid for case 2: a) axially extended and b) axially restricted.

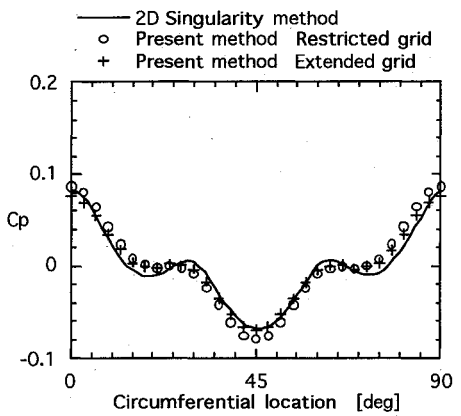

Fig. 7 Static pressure perturbation at the upstream boundary of restricted grid for case 2.

dius ratio to 0.99. For the purpose of validating the present method, the calculation results were compared with those produced by a two-dimensional singularity superposition method with Prandtl-Glauert transformation.[10] This singularity method has already been verified by comparing with experimental data for strut/pylon cascades. Figures 7 and 8 show C_p in the circumferential direction at the upstream and downstream boundary locations of restricted grid. Here, $N = 12$ and $L = 2$ were used in the Fourier-Bessel finite expansion. The use of the larger number did not improve the flow solutions in this case. A good agreement was obtained among the three kinds of calculations in each figure. Small differences among the results in Figs. 7 and 8 are possibly due to the second-order nonlinear effects.

The configurations and flow conditions treated in case 3 were similar to those of a bypass duct of typical turbofan engines, namely hub-to-tip radius ratio 0.6 and mean inlet

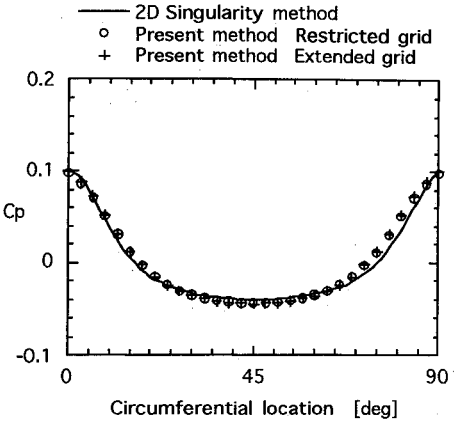

Fig. 8 Static pressure perturbation at the downstream boundary of restricted grid for case 2.

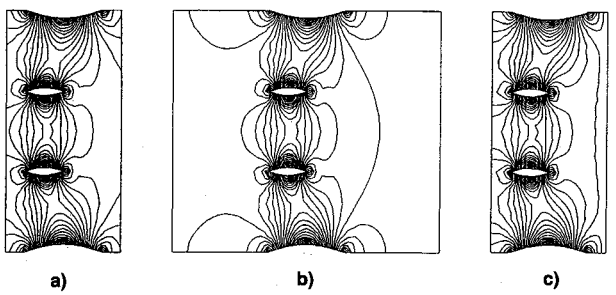

Fig. 9 Isopressure distribution at tip for case 3 (increments between isopressure lines are 1% of inlet stagnation pressure): a) nonreflecting boundary conditions on restricted grid, b) reflecting boundary conditions on extended grid, and c) reflecting boundary conditions on restricted grid.

number 0.52. Figure 9 shows the isopressure distribution at tip. The improvement by applying the present method was almost the same as that for case 1, qualitatively and quantitatively. The results at midspan or hub also indicate essentially the same behavior. $N = 12$ and $L = 10$ were large enough to obtain an acceptable solution.

The above results for cases 1–3 indicate that the present boundary conditions can allow a considerable reduction of the computational domain while maintaining the accuracy.

Conclusion

Three-dimensional nonreflecting boundary conditions regarding pressure waves and associated quantities have been formulated and applied to time-marching Euler equation calculations of steady flows around uncambered thick strut cascades. The numerical examples for the symmetric struts and the nonuniform strut cascades comprising two types of vanes have shown the correctness and accuracy of the present method, allowing a considerable reduction of the computational domain.

References

[1]Verdon, J. M., and Casper, J. R., "Subsonic Flow Past an Oscillating Cascade with Finite Mean Flow Deflection," *AIAA Journal*, Vol. 18, No. 5, 1980, pp. 540–548.

[2]Whitehead, D. S., "The Calculation of Steady and Unsteady Transonic Flow in Cascades," Cambridge Univ. Engineering Dept./A-Turbo/TR118, 1982.

[3]Hall, K. C., and Crawley, E. F., "Calculation of Unsteady Flows in Turbomachinery Using the Linearized Euler Equations," *Proceedings of the Fourth International Symposium on Unsteady Aerodynamics and Aeroelasticity of Turbomachines and Propellers*, 1987, pp. 15–38.

[4]Ferm, L., and Gustafsson, B., "A Down-Stream Boundary Procedure for the Euler Equations," *Computer and Fluids*, Vol. 10, No. 4, 1982, pp. 261–276.

[5]Hirsch, C., and Verhoff, A., "Far Field Numerical Boundary Conditions for Internal and Cascade Flow Computations," AIAA Paper 89-1943-CP, June 1989.

[6]Giles, M. B., "Non-Reflecting Boundary Conditions for Euler Equation Calculations," AIAA Paper 89-1942-CP, June 1989.

[7]Giles, M. B., "UNSFLO: A Numerical Method for Unsteady Inviscid Flow in Turbomachinery," Massachusetts Inst. of Technology Gas Turbine Lab., GTL Rept. 195, Cambridge, MA, 1988.

[8]Saxer, A. P., and Giles, M. B., "Quasi-3-D Non-Reflecting Boundary Conditions for Euler Equation Calculations," AIAA Paper 91-1603-CP, 1991.

[9]Denton, J. D., "An Improved Time-Marching Method for Turbomachinery Flow Calculation," American Society of Mechanical Engineers Paper 82-GT-239, 1982.

[10]Kodama, H., and Nagano, S., "Potential Pressure Field by Stator/Downstream Strut Interaction," *Journal of Turbomachinery*, Vol. 111, April 1988, pp. 197–203.